High-resolution Beijing MST radar detection of tropopause structure and variability over Xianghe (39.75° N, 116.96° E), China

Feilong Chen[1], Gang Chen[1*], Yufang Tian[2], Shaodong Zhang[1], Kaiming Huang[1], Chen Wu[1], Weifan Zhang[1]

[1]School of Electronic Information, Wuhan University, Wuhan 430072, China.

[2]Key Laboratory of Middle Atmosphere and Global Environment Observation, Institute of Atmospheric Physics, Chinese Academy of Sciences, Beijing 100029, China.

*Corresponding author: Gang Chen (g.chen@whu.edu.cn)

Abstract.

As a result of partial specular reflection from the atmospheric stable layer, the radar tropopause (RT) can simply and directly be detected by VHF radars with vertical incidence. Here, the Beijing MST radar measurements are used to investigate the structure and the variabilities of the tropopause in Xianghe, China with a temporal resolution of 0.5 hour from November 2011 to May 2017. High-resolution radar-derived tropopause is compared with the thermal lapse-rate tropopause (LRT) that defined by the World Meteorological Organization (WMO) criterion from twice daily radiosonde soundings and with the dynamical potential vorticity tropopause (PVT) that defined as the height of 2 PVU surface. During all the seasons, the RT and the LRT in altitude agree well with each other with a correlation coefficient of $\geq$0.74. Statistically, weaker (higher) tropopause sharpness seems to contribute to larger (smaller) difference between the RT and the LRT in altitude. The RT agrees well with the PVT in altitude during winter and spring with a correlation coefficient of $\geq$0.72, while the correlation

coefficient in summer is only 0.33. As expected, the monthly mean RT and LRT height both show seasonal variations. Lomb-Scargle periodograms show that the tropopause exhibits obvious diurnal variation throughout the seasons, whereas the semidiurnal oscillations are rare and occasionally observed during summer and later spring. Our study shows the ~~good capability~~potential of the Beijing MST radar to determine the tropopause height, as well as present its diurnal oscillations.

Key words: VHF radar; MST radar; tropopause; diurnal oscillation.

1. Introduction

The tropopause marks a transition zone separating the well-mixed convectively active troposphere from the stably stratified and more quiescent stratosphere. Its structure and variability is characterized by large changes in thermal (e.g., lapse rate), dynamical (e.g., potential vorticity), and chemical properties (e.g., ozone and water vapor) and hence acts as a key role for the stratosphere-troposphere exchange (STE) processes (Hoinka, 1998; Seidel et l., 2001). The height of the tropopause depends significantly on the latitude, with about 17 km near the equator and less than 9-10 km at polar latitudes (Ramakrishnan, 1933). Over subtropical latitudes with the presence of subtropical jet, where the tropopause experiences rapid change or breaking, tropopause folding events are commonly observed (Pan et al., 2004). Climatologically, the altitude of the tropopause represents the seasonal variation of the flux of stratospheric air intruding into the troposphere (Appenzeller et al., 1996). Moreover, the tropopause height trends can be a sensitive indicator of anthropogenic climate

change (Sausen and Santer, 2003; Santer et al., 2003a; Añel et al., 2006).

A variety of ways are available to determine the extratropical tropopause. Radiosonde sounding is the most commonly used to define the thermal tropopause (hereafter referred to as LRT) based on temperature lapse-rate (WMO, 1957). The thermal definition of tropopause can be applied globally and the tropopause height easily be determined from one individual profile (Santer et al., 2003). ~~Radiosonde sounding, however, is impracticable in severe weather conditions such as intense rainfall and cold air outbreak.~~ Another feasible definition is to use a specific potential vorticity (PV) surface to represent the dynamical tropopause (hereafter referred to as PVT) (Reed, 1955; Hoskins et al., 1985). Dynamical definition has the advantage that the PV is a conserved property (under adiabatic and friction-less conditions) of an air mass (Hoskins et al., 1985; Bethan et al., 1996). Values in the range 1-4 PVU (1 PVU= $10^6 \mathrm{m}^2 s^{-1} K kg^{-1}$ ~~$10^6\ m^2\ s^{-1}\ K\ kg^{-1}$~~) are used in previous researches in the Northern Hemisphere (e.g. Baray et al., 2000; Sprenger et al., 2003; Hoerling et al., 1991). The threshold of 2 PVU surface is the most commonly used (Gettelman et al., 2011). Dynamical definition, however, is not applicable near the equator, where the PV tends to be 0 (e.g., Hoerling et al., 1991; Nielsen-Gammon et al., 2001). Creating a blended tropopause globally may probably a good way forward (Wilcox et al., 2011). In addition, the data of GPS radio occultation satellites is also an effective way and commonly applied to study tropopause (e.g. Schmidt et al., 2005; Son et al., 2011).

As a result of partial specular reflection from stable atmospheric layer, the radar

68 tropopause (RT) can be well represented and identified by atmospheric radars operating
69 at meter wavelength (VHF band) and directing at vertical incidence (Gage and Green,
70 1979). Research activity increased remarkably following the first report on VHF radar
71 detection of tropopause by Gage and Green (1979), for instance, the researches in
72 middle latitudes (e.g. Hermawan et al., 1998), polar regions (e.g. Hall, 2013a), and
73 tropical regions (e.g. Das et al., 2008; Ravindrababu et al., 2014). Several methods have
74 been proposed to determine the tropopause height via radar echo power, including the
75 largest gradient in echo power (Vaughan et al., 1995; ~~Alexander et al., 2012~~ Alexander
76 et al., 2013), the maximum echo power (Vaughan et al., 1995; Hall et al., 2009), and
77 the specific value of echo power (Gage and Green, 1982; Yamamoto et al., 2003). The
78 method of the RT height determination used in this paper will be described in detail in
79 next section.

80 The biggest advantage of the VHF radar measurements is the ability of continuous
81 operation unmanned in any weather conditions. Of course, no definition of the
82 tropopause is perfect. VHF radar system can only be limited to a few locations globally.
83 A detailed review of the close relationship between these different tropopause
84 definitions is provided by Alexander et al., (2012).

85 By means of the radiosonde, reanalysis, and satellite data available globally, long-
86 term (annual or longer) variability in tropopause height has received extensive attention
87 (e.g. Randel et al., 2000; Angell and Korshover, 2009; Son et al., 2011; Liu et al., 2014).
88 However, short period (diurnal or semidiurnal) variability of the tropopause is hard to
89 be examined by these measurements. In contrast, benefiting from the much higher

temporal resolution, radar definition of the tropopause provides good capability for studying the diurnal and semidiurnal variation in tropopause height. Earlier, Yamamoto et al., (2003) reported the capability of the Equatorial Atmospheric Radar to examine the diurnal variation of tropopause height. Then, the diurnal variability of the tropical tropopause was investigated in detail by Das et al., (2008) using the Indian Gadanki MST radar. Its diurnal variation over a polar latitude station was investigated by Hall (2013b). In the absence of pressure and temperature parameters, the evidence of atmospheric tides can be well represented by winds (e.g. Huang et al., 2015).

The tropopause structure in midlatitudes is different from that in other regions. Double tropopauses structure is a ubiquitous feature over mid-latitude regions near 40°N (Pan et al., 2004; Randel et al., 2007). Strong evidence has revealed that the poleward intrusion of subtropical tropospheric air that occurred above the subtropical jet have resulted in the double structure (Pan et al., 2009). The higher part (second tropopause near ~16 km) is characterized by tropical features of cold and higher level, whereas the lower part (first tropopause near ~12 km) is characterized by polar features of warm and lower level. In the present study, we focus only on the first tropopause (below 16 km, if it exists) which will be referred to as 'tropopause' hereafter.

~~So far, knowledge on the high temporal resolution (within 1 hour) structure and variability of the midlatitude tropopause is still insufficient.~~ In this study, using more than 5 years of Beijing MST radar echo power measurements in vertical beam, we mainly focus on the high-resolution characteristics of the tropopause structure and their comparison with the simultaneous radiosonde and dynamical definitions. Another

important objective of this study is to examine the diurnal and semidiurnal variability of the tropopause. The observational characteristics of e.g. winds, echo power, and data acquisition rate near the tropopause layer are also presented in the paper.

2. Data and Methods

2.1. Radar Dataset

As an important part of the Chinese Meridian Project, two MST radar systems are designed and constructed to improve the understanding of the extratropical troposphere, lower stratosphere, and mesosphere (Wang, 2010), which are Wuhan and Beijing MST radars. The Beijing MST radar located in Xianghe, Hebei Province, China (39.75° N, 116.96° E, 22 m above sea level) was designed and constructed by the Institute of Atmospheric Physics, Chinese Academy of Sciences and started its routine operation since 20 October 2011 (Tian and Lu, 2017). The radar is a high power coherent pulse-Doppler radar operating at 50 MHz with the maximum peak power of 172 kW and the half-power beam width of 3.2°. Five beams are applied: one vertically pointed beam and four 15° off-zenith beams tilted to north, east, south, and west. In order to obtain the high-quality measurements from troposphere, lower stratosphere, and mesosphere simultaneously, the radar is designed to operate routinely in three separate modes: low mode (designed range 2.5-~12 km), middle mode (10-~25 km), and high mode (60-~90 km) with vertical resolutions of 150, 600, and 1200 m, respectively. Under the routine operation, the 15-min break is followed by the 15-min operation cycle (5 min for each mode). As a result, the time resolutions of the low, middle, and high mode

134 measurements are all 30 min. More detailed review of the radar system is given by
135 Chen et al. (2016).

136 Here only the low mode echo power measurements are used to determine the RT
137 height. Although the designed detectable range of the low mode is from 2.5-~12 km,
138 the vertically pointed beam can receive stronger echoes from a higher level (~14-15 km)
139 as compared with those from off-vertical beams due to the partial specular reflection
140 mechanism. The measurements in middle mode are also applied to calculate the winds
141 or echo power within ~5-6 km of the tropopause. The parameters for the two routine
142 operation modes are listed in Table 1. The monthly total number of the echo power
143 profiles available in vertical beam (low mode) is shown in Fig. 1. The outliers or
144 severely contaminated data that mainly induced by system problems are eliminated.
145 The large data gap in September is due to the annual preventive maintenance.

146 **2.2. Tropopause Definitions**

147 Due to the large gradient in potential temperature, radar return power received at
148 vertical incidence is significantly enhanced upon the transition zone of the tropopause
149 layer. Using this characteristic, the RT height can be determined effectively by the VHF
150 radar. Here, the RT is defined as the altitude (above 500 hPa) where the maximum
151 vertical gradient of echo power is located (Vaughan et al., 1995; ~~Alexander et al., 2012~~
152 Alexander et al., 2013; Ravindrababu et al., 2014; Chen et al., 2018). Considering the
153 occasional and random noise, to which the derived-RT is sensitive, the echo power
154 profiles are smoothed by a 3-point running mean. In order to further reduce the
155 influence of the noise, the RT definition used here need to satisfy an additional criterion:

the determined RT height should be continuous with the adjacent RT heights (one on each side), otherwise to search for the second peak gradient (eliminated if the second peak does not meet the additional criterion). The "continuous" here means that the discrepancy between the two successive heights (in time, 0.5-hour interval) should be <0.6 km. A typical example of the RT and LRT is illustrated in Fig. 2. The LRT is identified based on the World Meteorological Organization (WMO) criteria (WMO, 1957). The radar aspect sensitivity is expressed as the ratio between vertical (p_v) and oblique (p_o) beam echo power (here is 15° east beam). The radiosonde soundings are launched twice daily from the Beijing Meteorological Observatory (39.93 ºN, 116.28 ºE, station number 54511), which is less than 45 km to the radar site. In this case, the LRT and RT consistent well and are at 11.65 km and 11.85 km respectively. As expected, the LRT characterized by a rapid increase in potential temperature gradient also corresponds to the large gradient in radar aspect sensitivity. Note that the height with maximum value in echo power lie at a higher altitude (as compared with the RT height) of ~700 m above the LRT. The dynamical tropopauses used in this paper are derived from the European Centre for Medium-Range Weather Forecasts (ECMWF) ERA-Interim Reanalysis (Dee et al., 2011) and defined as the surface of 2 PVU potential vorticity, which is same to that used by Sprenger et al., (2003) and Alexander et al. (~~2012~~2013).

2.3. Tropopause sharpness definition

For the compared data pairs between the RT and LRT, we calculate the corresponding tropopause sharpness that represents the strength of the tropopause

inversion layer. As defined by Wirth, (2000), the tropopause sharpness S_{TP} can be calculated as:

$$S_{TP} = \frac{T_{TP+\Delta Z} - T_{TP}}{\Delta Z} - \frac{T_{TP} - T_{TP-\Delta Z}}{\Delta Z} \quad (1)$$

where TP denotes the tropopause height, $\Delta Z = 1$ km, and T_{TP} indicates the corresponding temperature. This definition is also used in Alexander et al. 2013 and we're using it for a good comparison with our results.

3. Results

3.1. High-resolution radar tropopause structure

The height-time cross section of radar echo power and aspect sensitivity is shown in Fig. 3 for a typical month (February 2014), along with the RT, PVT and LRT marked in the figure. In general, the RT agreed well with both the LRT and PVT in height, and most of the RT exhibit a slightly higher altitude. However, the differences between the RT and LRT are sometimes large (reach to ~1-2 km) especially when the RT experience rapid change. Regardless of the background synoptic condition, the difference in the definitions themselves is to a large degree the main contributing factor for the large difference between the RT and LRT. For example, a second layer with significant enhanced echo power is observed above the radar-derived RT for the cases on 4 and 5 February 2012 (Fig.3a). According to the definitions, the RT is well defined as the first layer with echo enhanced echo power and the LRT matched the second

layer, similar to that observed by Yamamoto et al., (2003) and Fukao et al., (2003). It is of note that the RT well separates the troposphere characterized by low aspect sensitivity from the lower-stratosphere characterized by high aspect sensitivity (Fig.3b).

3.2. Comparisons between different definitions

To further quantify the consistency and difference in altitude between different tropopause definitions, a detailed comparison is carried out in this section. The seasonal scatterplots for RT versus LRT and the histogram distribution of altitude differences between the RT and LRT are illustrated in Fig. 4, during the period November 2011-May 2017. A total of 2411 data pairs are obtained for comparison. Among them, the number of data pairs is 845 for DJF (winter), 721 for MAM (spring), 321 for JJA (summer), and 524 for SON (autumn). Comparisons have shown a good consistency throughout the seasons and most of the RTs exhibit a slightly higher than the LRTs. The correlation coefficient is 0.74, 0.80, 0.82, and 0.78 for DJF, MAM, JJA, and SON, respectively. The mean and standard deviation difference (RT minus LRT) calculated in DJF, MAM, JJA, and SON is (0.14 ± 0.75), (0.26 ± 0.78), (0.33 ± 0.56), and (0.12 ± 0.69) km, respectively. The proportion of the data pairs with differences <500 m is reasonably good during four seasons and is 63%, 61%, 64%, and 67% for DJF, MAM, JJA, and SON, respectively. Fig. 4 explicitly ~~indicates the good capability~~shows that the RT derived by ~~of~~ the Beijing MST radar ~~to determine~~agrees reasonably well with the ~~tropopause structure well~~LRT throughout the seasons.

To examine the potential role of the sharpness, Fig. 5a and Fig. 5b show the histogram distribution of the tropopause sharpness along with the probability density

curve for data pairs with difference (absolute values of RT minus LRT) <0.5 km and >1 km respectively. What is apparent is that most data pairs of Fig. 5a are located to the right (higher sharpness values, with the peak of ~7.06 K/km) and of Fig. 5b are to the left (lower sharpness values, with the peak of ~6.35 K/km). No matter whether this distribution feature is associated with the cyclonic-anticyclonic systems (e.g. Randel et al., 2007; Randel and Wu, 2010), the results more or less demonstrate that the larger (weaker) tropopause sharpness contribute to lower (higher) difference between the RT and LRT. From the perspective of seasonal statistics, the tropopause sharpness over Beijing station shows similar distribution characteristics throughout the seasons (not shown), which is different from that in polar regions where the sharpness is significantly higher during summer than during winter (Zängl and Hoinka, 2001).

The seasonal scatterplots and height difference distribution between the RT and PVT are illustrated and quantified in Fig. 6. The total number of comparing data pairs for winter, spring, summer, and autumn is 1422, 1260, 791, and 1145, respectively. During winter and spring (Fig. 6a and 6b), the RTs agree reasonably well with the PVTs with the correlation coefficient of 0.72 and 0.76 and the mean difference (RT minus PVT) of (0.55± 0.84 km) and (1± 0.89 km), respectively. In contrast, the consistency for summer and autumn (Fig. 6c and 6d) is relatively bad and with correlation coefficient of 0.33 and 0.47 and mean difference of (0.80± 1.39 km) and (0.75± 1.23 km), respectively. Especially for summer, the proportion of the comparing data pairs with difference <0.5 km is only 10.6% (84). In autumn, need to note that most data pairs with poor consistency is sampled during early autumn.

3.3. Observational characteristics in the vicinity of ~~the~~ tropopause

Measurements of radar middle mode are used for examining the horizontal wind, return power, and effective wind data acquisition rate within 5-6 km of the tropopause (upper troposphere and lower stratosphere). Left panels of Fig. 7 show the vertical scatterplots of the static stability (represented by the buoyancy frequency squared) as a function of height relative to the LRT and the right panels show the radar echo power as a function of height relative to the RT, during two specific years 2012-2013 for extended winter NDJFM and summer MJJAS seasons. Mean and standard deviations are also plotted in each panel of Fig. 7. As expected, ~~Results~~ results clearly ~~demonstrate the~~show sudden jump in static stability and ~~rapid increase in echo~~ radar power ~~upon~~ near the ~~corresponding~~ tropopause layer. The degree of sudden increase~~variation~~ in echo power is more gradual than that in static stability. T~~T~~he amplitude of ~~both the jump and~~ the sudden increase in radar power experienced a slightly larger during NDJFM than that during MJJAS (red lines of right panels). Another interesting feature in the lower-stratosphere is that both the static stability and radar power points show less disperse during NDJFM than that during MJJAS.

Fig. 8 shows the profiles of mean radar effective wind data acquisition rate for low and middle modes during November 2011-May 2017. Clearly, both ~~Here, the "effective data" of one specific range gate requires at least three non-coplanar beams have received backscattered echoes, by which 3-dimensional wind can be derived. The mean data acquisition rate p~~profiles ~~both~~ exhibit ~~an obvious inversion layer (i.e.~~a sudden increase ~~significantly~~ with height~~)~~ near the tropopause, with the first peak located ~1

km higher above the mean tropopause height. Note that the second inversion in middle mode profile that occurred near 16 km is associated with the second tropopause. As limited by the highest detectable altitude (the data acquisition rate decreased to lower than 20% at ~16 km), the profile in low mode shows little evidence of second inversion.

Fig. 9 shows time-height intensity plot of the monthly mean radar-derived horizontal wind (from middle mode) during November 2011-May 2017, together with the monthly mean location of RT and LRT. One pixel grid denotes 1 month×0.6 km. The monthly mean RT and LRT agreed well with each other in height, within 400 m in August and September and even lower in other months of about within 200 m. They both exhibit a clear seasonal variation, with maximum in early autumn of ~11.6 km and minimum in early spring of ~10.3 km. The monthly mean wind jet varies with season, with the thinnest thickness and lowest strength in summer. The mean tropopause height appears to correspond to the lower boundary location of peak wind layer. The error bars of both the RT and LRT help to illustrate that the tropopauses changes by larger amplitude in winter and June than that in other months.

3.4. Periodogram analysis of the radar tropopause

High temporal resolution detection of tropopause by VHF radar have allowed us to investigate the diurnal or semidiurnal variability of the tropopause. Atmospheric tides are well known global oscillations contributing to the diurnal variation in temperature and background winds, which in turn modulate the tropopause height. With the absence of ~~high resolution~~ temperature measurements, ~~radar-derived wind~~zonal and meridional ~~s~~ winds are ~~combined used~~applied to ~~represent~~ demonstrate the evidence of diurnal or

semidiurnal ~~variation in tropopause height that~~ modulate~~d~~ion by tidal. The frequency power spectrum of the RT height, zonal and meridional wind, calculated by means of Lomb-Scargle method (Press and Rybicki, 1989), is illustrated in Fig. 10 for two typical months: May 2015 and December 2016. The choice of Lomb-Scargle algorithm is due to the presence of data gaps (~2 days per week, especially during 2012-2013). The dominant ~24 h periodicity in RT height, zonal and meridional wind is obvious for both months. The evidence of ~12 h period in all three parameters is distinct for May 2015 (Fig. 10a), although the power is relatively weaker. Through the analysis for each individual month, we found that the semidiurnal component in the three parameters is generally and occasionally observed in summer and later spring during our experimental period. The characteristics of the diurnal variation of the RT height can be represented better in Fig. 11, which shows the mean Lomb-Scargle power spectrum of the RT as a function month during November 2011-May 2017. As compared with other months, the dominant diurnal periodicity is less evident in April. We need to clarify that atmospheric tides are of course not the only source of the diurnal variation in tropopause height, diurnal convective activities (Yamamoto et al., 2003) might also be an important cause. Here will not be ~~detailly~~ discussed in detail.

4. Discussion

As for the radar echo power definition, the RT estimation sometimes will fail due to the system problems, even if the thermal tropopause is well defined (Hall et al., 2009). Apart from the system problems (e.g. the damage of T/R module), the following two

conditions are primarily responsible for the failure (or difficulty) of both the radar and thermal definitions over the radar site latitude (~40° N). Firstly, the temperature sometimes continued to decrease ~~upon into~~until to ~~the~~ the ~~lower~~ stratosphere (~~below~~ above 16 km) in summer and early autumn, leading to the failure/difficulty of both the radar and thermal definitions (a typical case as shown in Fig. 12a). Need to note that the temperature inversion layer occurred at ~16 km in summer or early autumn is the second tropopause with characteristics of Tropics (Pan et al., 2004; Randel et al., 2007). Secondly, some specific meteorological processes can lead to the ambiguities and indefiniteness in thermal and radar definitions, such as fronts, cyclones or typhoons, and folding (e.g. Nastrom et al., 1989; May et al., 1991; Roettger, 2001; Alexander et al., 2013). Such ambiguities often result in large difference in altitude between the RT and LRT. ~~Especially~~ In addition, when multiple temperature inversion layers occurred (below 16 km), the RT ~~generally~~ sometimes matched the lower layer ~~part~~ with enhanced echo power and LRT often matched the upper ~~part~~ layer (e.g. Yamamoto et al., 2003; Fukao et al., 2003)~~, such as the double layers of enhanced echo power shown in Fig. 3 on 4 and 5 February 2012~~. Apart from the ~~two~~ situations above, ~~there is~~ another condition ~~that~~ is also commonly responsible for the difficult in identifying the thermal tropopause from radiosonde profiles during summer~~failure of thermal definition in summer and early autumn~~. As ~~the~~ a typical case shown in Fig. 12b, a significant inversion in temperature (at ~12 km) is recorded from the radiosonde profile, but ~~this~~ the altitude extent of inversion layer is too thin to meet the WMO criterion ~~inversion layer is too thin and weak to meet the WMO criterion~~ that thermal definition required.

Whereas, the apparent enhancement in radar echo power corresponding to such inversion layer is strong enough to well define the RT. ~~Need to highlight again that t~~The temperature inversion ~~layer~~located near ~16 km (the second tropopause) ~~that occurred near ~16 km is the second tropopause (~~is not ~~considered here~~the focus of this paper~~)~~. ~~The conditions mentioned above are the main reasons for fewer comparison data pairs in summer than that in other seasons (Fig. 4c and Fig. 6c).~~

Pan et al., (2004) have reported that the difference between the LRT and PVT are more distinct in the vicinity of subtropical jet. In the northern hemisphere, the axis of the subtropical jet is situated near ~30°N in spring and winter, whereas in summer and early autumn the subtropical jet shifts northward to ~40°N (see Fig. 4 in Ding and Wang, 2006). We preliminary considered that the ~~bad~~ inconsistency between the RT and PVT in summer and early autumn (Fig. 6c and 6d) is most likely ~~associated with~~related to the subtropical jet shifting poleward to ~40°N. The existing cyclones or anticyclones in the upper-troposphere (Wirth, 2000), of course, may also be an important influence factor for the~~cause of the~~ significant asymmetric differences (most of the scattered points deviate significantly from the 1:1 line). ~~(~~The asymmetric differences, that is ~~scattered points deviate significantly from the 1:1 line and PVT located below the RT in most cases~~most of the RT are located higher than the 2PVU tropopause height~~, as shown in Fig. 6c)~~, suggest that the 2PVU surface is not the best measure of a dynamical tropopause over Beijing during summer-time. More detailed discussion about the striking asymmetric differences in height between LRT and PVT can be seen in Wirth (2001) and will not be given here. Anyway, we need to be careful when using the 2PVU

dynamical definition to define the tropopause over radar site latitude ~40° N, especially in summer.

About the characteristics of tropopause and the comparison between different definitions, there are many differences between mid-latitude and polar regions. In mid-latitude (~40°N), our results show that: (1) the agreement between RT and LRT is similar good throughout the seasons; (2) RTs are generally located higher than the LRT; (3) the thermal definition sometimes fail in summer and early autumn; (4) the agreement between the RT/LRT and PVT in summer is poor. Whereas, in contrast, previous researches about the tropopause over polar regions ~~showed~~ reported that (Wirth, 2000；~~Alexander et al., 2012~~ Alexander et al., 2013): (1) the difference between the RT and LRT is larger during winter than that during summer; (2) RTs are generally located lower than the LRT; (3) the thermal definition sometimes fail in winter and spring; (4) the comparison between the RT and PVT showed the similar good agreement during both summer and winter.

Over a polar latitude station, the seasonal characteristics of the diurnal oscillation in tropopause height were investigated using 5 years of SOUSY VHF radar measurements (Hall, 2013b). The sunlight variability in polar regions is different from that in other latitudes of the world. Different sunlight variation actually will lead to difference in atmospheric tides, and then would result in different diurnal variation in tropopause height. Here we found that the diurnal oscillation of RT height at Xianghe is ubiquitous and obvious throughout the seasons except for April (Fig. 11). Whereas at polar latitude and in months of November to February when there is no sunlight, Hall

(2013b) observed little evidence of 24 h diurnal variability in RT height.

5. Conclusions

In this paper, we present the high resolution structure and variability of the tropopause in Xianghe, China (39.75° N, 116.96° E), based on the Beijing MST radar vertical beam echo power data collected during the period November 2011-May 2017. Fine-scale structure of the RT is well determined with a high temporal resolution of 0.5 h. Comparison results have shown good agreement in altitude between the RT and LRT, with a correlation coefficient of ≥ 0.74 for the four seasons. Higher tropopause sharpness seems to contribute lower difference between the RT and LRT in altitude and weaker sharpness appears responsible for higher difference. The agreement between the RT and PVT is relatively well in winter and spring with correlation coefficient of 0.72 and 0.76 respectively, but poor during summer with a correlation coefficient of only 0.33. We initially suggested that the poor consistency between RT and PVT is associated with the subtropical jet shifting poleward to ~40°N.

As expected, the sudden jump in static stability (represented by the buoyancy frequency squared) and the rapid increase in radar echo power upon the tropopause layer are clearly observed. Upon the tropopause layer, ~~A~~ a ~~significant inversion (increasing with height)~~sudden increase in effective radar data acquisition rate is also observed ~~upon the tropopause layer~~. Both the monthly mean RT and LRT height have shown a clear annual cycle. The variability and oscillation of RT height with diurnal or lower timescales is presented. Obvious diurnal variation in tropopause height, zonal

wind, and meridional wind is generally observed throughout the seasons, indicating the modulation most likely from the atmospheric tides. The semidiurnal variation in RT height is not so obvious and commonly observed occasionally in summer and late spring.

Acknowledgment

This work is funded by National Natural Science Foundation of China (NSFC grants No. 41474132 and 41722404). We acknowledge the Chinese Meridian Project for providing the MST radar data. The authors sincerely acknowledge the ECMWF for providing global reanalysis data. The MST radar data for this paper are available at Data Centre for Meridian Space Weather Monitoring Project (http://159.226.22.74/). The radiosonde data are publicly available from the NOAA/ESRL Database at https://ruc.noaa.gov/raobs/.

References

Alexander, S.P., Murphy, D.J., and Klekociuk, A.R.: High resolution VHF radar measurements of tropopause structure and variability at Davis, Antarctica (69◦ S, 78◦ E), Atmos. Chem. Phys., 13, 3121-3132, 2013.~~Alexander, S. P., Murphy, D. J., and Klekociuk, A. R.: High resolution VHF radar measurements of tropopause structure and variability at Davis, Antarctica (69º S, 78º E). Atmospheric Chemistry and Physics, 12(10), 26173-26205, 2012.~~

419 Angell, J. K., and Korshover, J.: Quasi-biennial and long-term fluctuations in
420 tropopause pressure and temperature, and the relation to stratospheric water vapor
421 content. Monthly Weather Review, 102(1), 29-34, 2009.
422 Appenzeller, C., Holton, J. R., and Rosenlof, K. H.: Seasonal Variation of Mass
423 Transport Across the Tropopause. Journal of Geophysical Research, 101(D10),
424 15071-15078, 1996.
425 Añel, J. A., J. C. Antuña, L. de la Torre, R. Nieto, and Gimeno L.: Changes in
426 tropopause height for the Eurasian region determined from CARDS radiosonde
427 data. Naturwissenschafte, 93, 603–609, doi:10.1007/s00114-006-0147-5, 2006.
428 Bethan, S., Vaughan, G., and Reid, S. J.: A comparison of ozone and thermal tropopause
429 heights and the impact of tropopause definition on quantifying the ozone content
430 of the troposphere. Quarterly Journal of the Royal Meteorological Society,
431 122(532), 929-944, 1996.
432 Baray, J., Daniel, V., Ancellet, G., and Legras, B.: Planetary-scale tropopause folds in
433 the southern subtropics. Geophysical Research Letters, 27(3), 353-356, 2000.
434 Chen, F. L., Chen, G., Shi, C. H., Tian, Y. F., Zhang, S. D., and Huang, K. M.: Strong
435 downdrafts preceding rapid tropopause ascent and their potential to identify cross-
436 tropopause stratospheric intrusions, Annales Geophysicae, 36(5), 1403-1417,
437 2018.
438 Chen, G., Cui, X., Chen, F., Zhao, Z., Wang, Y., Yao, Q., and Gong, W.: MST Radars
439 of Chinese Meridian Project: System Description and Atmospheric Wind
440 Measurement. IEEE Transactions on Geoscience and Remote Sensing, 54(8),

441 4513-4523, 2016.
442 Das, S. S., Jain, A. R., Kumar, K. K., and Rao, D. N.: Diurnal variability of the tropical
443 tropopause: Significance of VHF radar measurements. Radio Science, 43(6), 1-14,
444 doi:10.1029/2008RS003824, 2008.
445 Dee, D. P., Uppala, S. M., Simmons, A. J., Berrisford, P., Poli, P., Kobayashi, S. et al.:
446 The ERA-Interim reanalysis: configuration and performance of the data
447 assimilation system. Quarterly Journal of the Royal Meteorological Society,
448 137(656), 553-597, 2011.
449 Ding, A., and Wang, T.: Influence of stratosphere-to-troposphere exchange on the
450 seasonal cycle of surface ozone at Mount Waliguan in western China. Geophysical
451 Research Letters, 33(3), 233-252, doi:10.1029/ 2005GL024760, 2006.
452 Fukao, S., H. Hashiguchi, M. Yamamoto, T. Tsuda, T. Nakamura, M. K. Yamamoto,
453 T. Sato, M. Hagio, and Y. Yabugaki:. Equatorial Atmosphere Radar (EAR):
454 System description and first results. Radio Science, 38(3), 1053, 2003.
455 Gage, K. S., and Green, J. L.: An objective method for the determination of tropopause
456 height from VHF radar observations. Journal of Applied Meteorology, 21(21),
457 1150-1154, 1982.
458 Gage, K. S., and Green, J. L.: Tropopause Detection by Partial Specular Reflection with
459 Very-High-Frequency Radar. Science, 203(4386), 1238-1240, 1979.
460 Gettelman, A., P. Hoor, L. L. Pan, W. J. Randel, M. I. Hegglin, and T. Birner: The
461 extratropical upper troposphere and lower stratosphere, Reviews of Geophysics,
462 49(3), RG3003, doi: 10.1029/2011RG000355, 2011.

463 Hermawan, E., Tsuda, T., and Adachi, T.: MU radar observations of tropopause
464 variations by using clear air echo characteristics. Earth, Planets and Space, 50(4),
465 361-370, 1998.
466 Hall, C.: The radar tropopause above Svalbard 2008–2012: Characteristics at various
467 timescales. Journal of Geophysical Research, 118(6), 2600-2608, 2013a.
468 Hall, C.: The radar tropopause at 78°N, 16°E: Characteristics of diurnal variation.
469 Journal of Geophysical Research, 118(12), 6354-6359, doi:10.1002/jgrd.50560,
470 2013b.
471 Hall, C. M., Röttger, J., Kuyeng, K., Sigernes, F., Claes, S., and Chau, J. L.: Tropopause
472 altitude detection at 78°N, 16°E, 2008: First results of the refurbished SOUSY
473 radar. Radio Science, 44(5), 1-12, doi:10.1029/ 2009RS004144, 2009.
474 Hoinka, K. P.: Statistics of the Global Tropopause Pressure. Monthly Weather Review,
475 126(12), 3303-3325, 1998.
476 Hoskins, B. J., Mcintyre, M. E., and Robertson, A. W.: On the use and significance of
477 isentropic potential vorticity maps. Quarterly Journal of the Royal Meteorological
478 Society, 111(470), 877-946, 2007.
479 Huang, C., Zhang, S. D., Zhou, Q. H., Yi, F., Huang, K., Gong, Y., Zhang, Y., and Gan,
480 Q.: WHU VHF radar observations of the diurnal tide and its variability in the lower
481 atmosphere over Chongyang (114.14° E, 29.53° N), China. Annales Geophysicae,
482 33(7), 865-874, 2015.
483 Hoerling, M. P., Schaack, T. K., and Lenzen, A. J.: Global Objective Tropopause
484 Analysis. Monthly Weather Review, 119(8), 1816-1831, 1991.

485 Liu, Y., Xu, T., and Liu, J.: Characteristics of the seasonal variation of the global
486 tropopause revealed by cosmic/GPS data. Advances in Space Research, 54(11),
487 2274-2285, 2014.
488 May, P. T., Yamamoto, M., Fukao, S., Sato, T., Kato, S., and Tsuda, T.: Wind and
489 reflectivity fields around fronts observed with a VHF radar. Radio Science, 26(5),
490 1245-1249, 1991.
491 Nastrom, G. D., Green, J. L., Gage, K. S., and Peterson, M. R.: Tropopause Folding
492 and the Variability of the Tropopause Height as Seen by the Flatland VHF Radar.
493 Journal of Applied Meteorology, 28(12), 1271-1281, 1989.
494 Nielsen-Gammon, J. W.: A visualization of the global dynamic tropopause. Bulletin of
495 the American Meteorological Society, 82(6), 1151-1168, 2001.
496 Pan, L. L., Randel, W. J., Gary, B. L., Mahoney, M. J., and Hintsa, E. J.: Definitions
497 and sharpness of the extratropical tropopause: A trace gas perspective. Journal of
498 Geophysical Research, 109, D23103, doi:10.1029/2004JD004982, 2004.
499 Pan, L. L., W. J. Randel, J. C. Gille, W. D. Hall, B. Nardi, S. Massie, V. Yudin, R.
500 Khosravi, P. Konopka, and D. Tarasick: Tropospheric intrusions associated with
501 the secondary tropopause, Journal of Geophysical Research, 114, D10302, 2009.
502 Press, W. H., and Rybicki, G. B.: Fast algorithm for spectral analysis of unevenly
503 sampled data. The Astrophysical Journal, 338(1), 277-280, 1989.
504 Ravindrababu, S., Venkat Ratnam, M., Sunilkumar, S. V., Parameswaran, K., and
505 Krishna Murthy, B. V.: Detection of tropopause altitude using Indian MST radar
506 data and comparison with simultaneous radiosonde observations. Journal of

507 Atmospheric and Solar-Terrestrial Physics, 121(6), 679-687, 2014.
508 Randel, W. J., Wu, F., and Gaffen, D. J.: Interannual variability of the tropical
509 tropopause derived from radiosonde data and NCEP reanalyses. Journal of
510 Geophysical Research Atmospheres, 105(D12), 15509-15523, 2000.
511 Randel, W. J., Seidel, D. J., and Pan, L. L.: Observational characteristics of double
512 tropopauses. Journal of Geophysical Research, 112, D07309, 2007.
513 Randel, W. J., and Wu, F.: The Polar Summer Tropopause Inversion Layer. Journal of
514 the Atmospheric Sciences, 67(8), 2572-2581, 2010.
515 Randel, W. J., Wu, F., and Forster, P. M.: The extratropical tropopause inversion layer:
516 Global observations with GPS data, and a radiative forcing mechanism. Journal of
517 the Atmospheric Sciences, 64(12), 4489-4496, 2007.
518 Ramakrishnan, K. P.: Distortion of the tropopause due to meridional movements in the
519 sub-stratosphere. Nature, 132(3346), 932-932, 1933.
520 Roettger, J.: Observations of the polar d-region and the mesosphere with the Eiscat
521 Svalbard radar and the SOUSY Svalbard Radar (scientific paper). Memoirs of
522 National Institute of Polar Research. Special Issue, 54(94), 9-20, 2001.
523 Reed, R. J.: A study of a characteristic tpye of upper-level frontogenesis. Journal of the
524 Atmospheric Sciences, 12(3), 226-237, 1955.
525 Santer, B. D., Wehner, M. F., Wigley, T. M., Sausen, R., Meehl, G. A., Taylor, K. E.,
526 Ammann, C., Arblaster, J., Washington, W. M., Boyle, J. S., and Brüggemann, W.:
527 Contributions of anthropogenic and natural forcing to recent tropopause height
528 changes. Science, 301(5632), 479-483, 2003.

Santer, B. D., Sausen, R., Wigley, T. M., Boyle, J. S., Achutarao, K., Doutriaux, C., Hansen, J. E., Meehl, G. A., Roeckner, E., Ruedy, R., Schmidt, G., and Taylor, K. E.: Behavior of tropopause height and atmospheric temperature in models, reanalyses, and observations: Decadal changes. Journal of Geophysical Research, 108(D1), 4002, doi:10.1029/2002JD002258, 2003a.

Sausen, R., and Santer, B. D.: Use of Changes in Tropopause Height to Detect Human Influences on Climate. Meteorologische Zeitschrift, 12(3), 131-136, 2003.

Schmidt, T., Heise, S., Wickert, J., Beyerle, G., & Reigber, C.: GPS radio occultation with CHAMP and SAC-C: global monitoring of thermal tropopause parameters. Atmospheric Chemistry and Physics, 5(6), 1473-1488, 2005.

Seidel, D. J., Ross, R. J., Angell, J. K., and Reid, G. C.: Climatological characteristics of the tropical tropopause as revealed by radiosondes. Journal of Geophysical Research, 106(D8), 7857-7878, 2001.

Son, S. W., Tandon, N. F., & Polvani, L. M.: The fine-scale structure of the global tropopause derived from COSMIC GPS radio occultation measurements. Journal of Geophysical Research: Atmospheres, 116(D20), 2011.

~~Son, S., Tandon, N. F., and Polvani, L. M.: The fine-scale structure of the global tropopause derived from cosmic gps radio occultation measurements. Journal of Geophysical Research Atmospheres, 116, D20113, 2011.~~

Sprenger, M., Croci Maspoli, M., and Wernli, H.: Tropopause folds and cross-tropopause exchange: a global investigation based upon ECMWF analyses for the

time period March 2000 to February 2001. Journal of Geophysical Research Atmospheres, 108(12), 291-302, 2003.

Tian, Y., and Lu, D.: Comparison of Beijing MST Radar and Radiosonde Horizontal Wind Measurements. Advances in Atmospheric Sciences, 34(1), 39-53. doi: 10.1007 / s00376-016-6129-4, 2017.

Vaughan, G., Howells, A., and Price, J. D.: Use of MST radars to probe the mesoscale structure of the tropopause. Tellus A, 47(5), 759-765, 1995.

Wang, C.: Development of the Chinese meridian project. Chinese Journal of Space Science, 30(4), 382–384, 2010.

Wilcox L.J., Hoskins B.J., Shine K.P. 2012. A global blended tropopause based on ERA data. Part I: Climatology. Q. J. R. Meteorol. Soc. 138: 561–575. DOI:10.1002/qj.951.

Wirth, V.: Thermal versus dynamical tropopause in upper-tropospheric balanced flow anomalies. Quarterly Journal of the Royal Meteorological Society, 126(562), 299-317, 2000.

Wirth, V.: Cyclone-anticyclone asymmetry concerning the height of the thermal and the dynamical tropopause. Journal of the Atmospheric Sciences, 58(1), 26-37, 2001.

WMO: Definition of the tropopause. WMO Bull., 6, 136, 1957.

Yamamoto, M., Oyamatsu, M., Horinouchi, T., Hashiguchi, H., and Fukao, S.: High time resolution determination of the tropical tropopause by the Equatorial Atmosphere Radar. Geophysical Research Letters, 30(21), 2094, 2003.

572 Zängl, G., and Hoinka, K. P.: The tropopause in the polar regions. Journal of Climate,
573 14(2001), 3117-3139, 2001.
574

575 **Table**

Radar parameter	Value
Transmitted frequency	50 MHz
Antenna array	24×24 3-element Yagi
Antenna gain	33 dB
Transmitter peak power	172 kW
Code	16-bit complementary
No. coherent integrations	128 (low mode)/64 (mid mode)
No. FFT points	256
No. spectral average	10
Pulse repetition period	160 (low mode)/320 (mid mode) μs
Half power beam width	3.2^o
Pulse length	1 (low mode)/4 (mid mode) μs
Range resolution	150 (low mode)/600 (mid mode) m
Temporal resolution	30 min
Off-zenith angle	15^o

576 **Table 1.** Routine operational parameters in low and middle mode for the Beijing MST
577 radar used in this study.

578

Figures

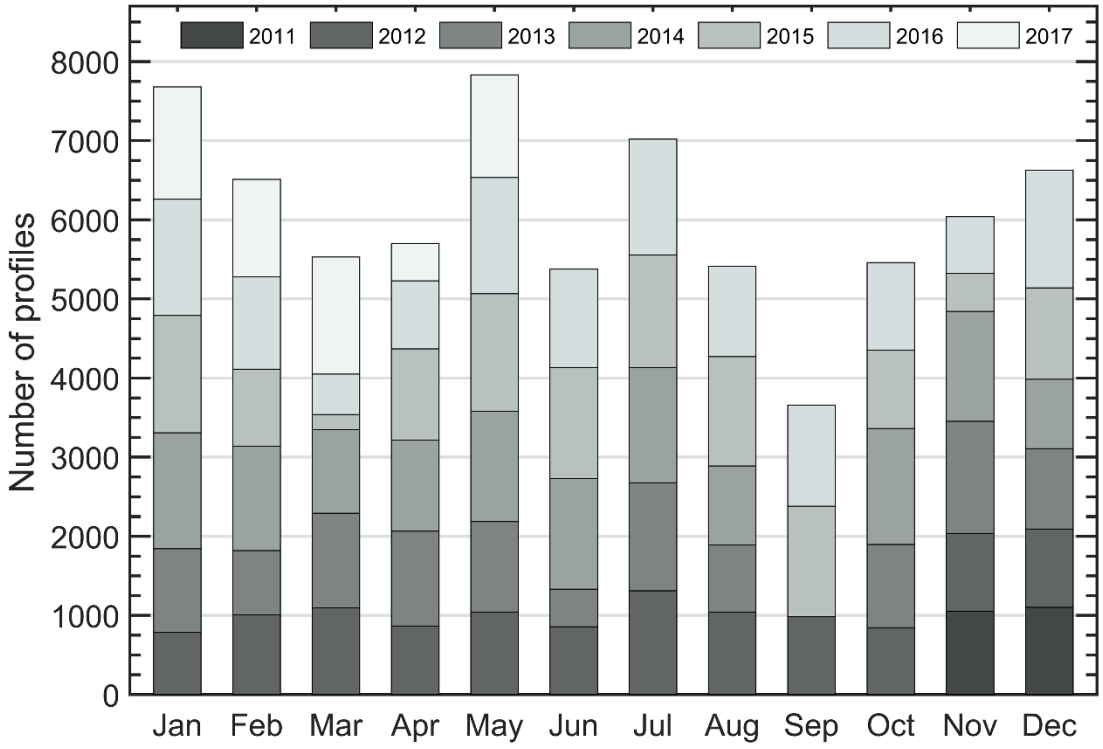

Figure 1. Distribution of the monthly total number of radar return echo power profiles that available from vertical beam in low mode, collected for the period November 2011-May 2017.

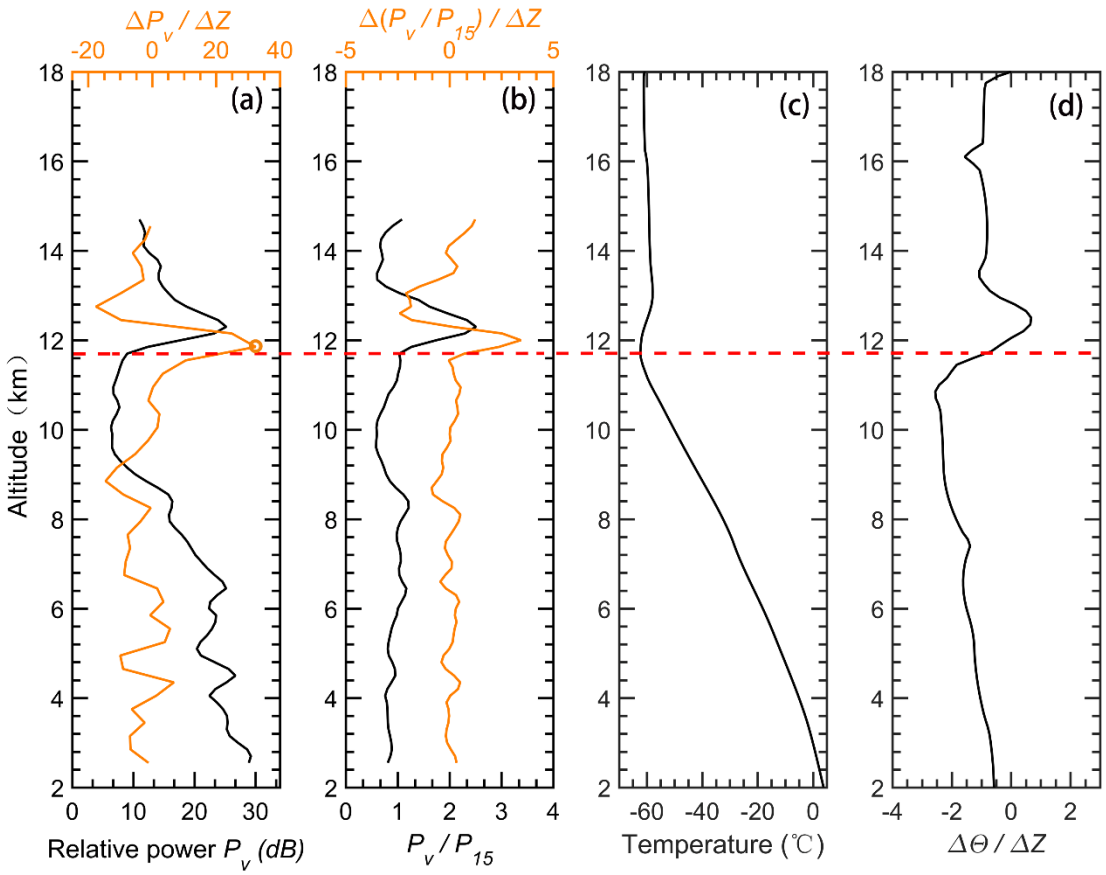

584

585 **Figure 2.** Example vertical profiles of (a) relative radar echo power (black line) along

586 with its gradient variation (orange line), (b) radar aspect sensitivity (black line) along

587 with its gradient variation (orange line), (c) radiosonde temperature and (d) potential

588 temperature gradient on 00 UT 04 November 2011. The horizontal red dashed line

589 marks the LRT height. The orange circle in Fig. 2a denotes the RT height.

590

591

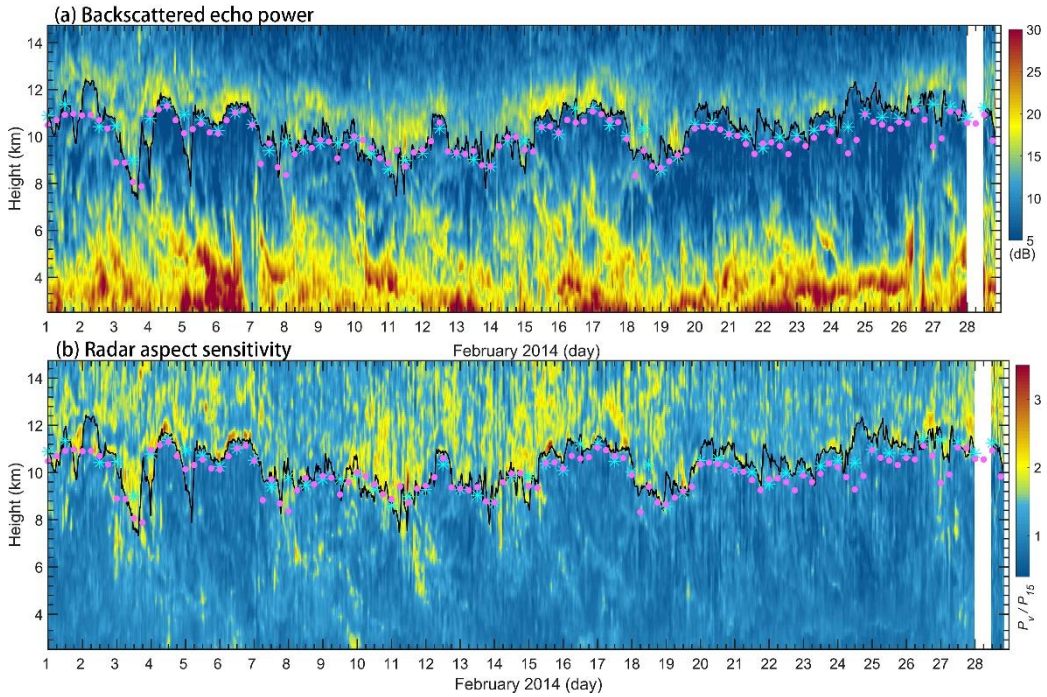

592

593 **Figure 3.** Altitude-time intensity plot of (a) radar backscattered echo power and (b)

594 radar aspect sensitivity for February 2014. The tropopauses determined based on the

595 radar echo definition are shown as a black solid curve. The ~~green~~ cyan asterisks '*' and

596 pink dots indicate the location of the LRT derived from simultaneous twice daily

597 radiosonde data and the PVT from ECMWF ERA-Interim reanalysis, respectively.

598 White stripe indicates the time frame of radar missing data.

599

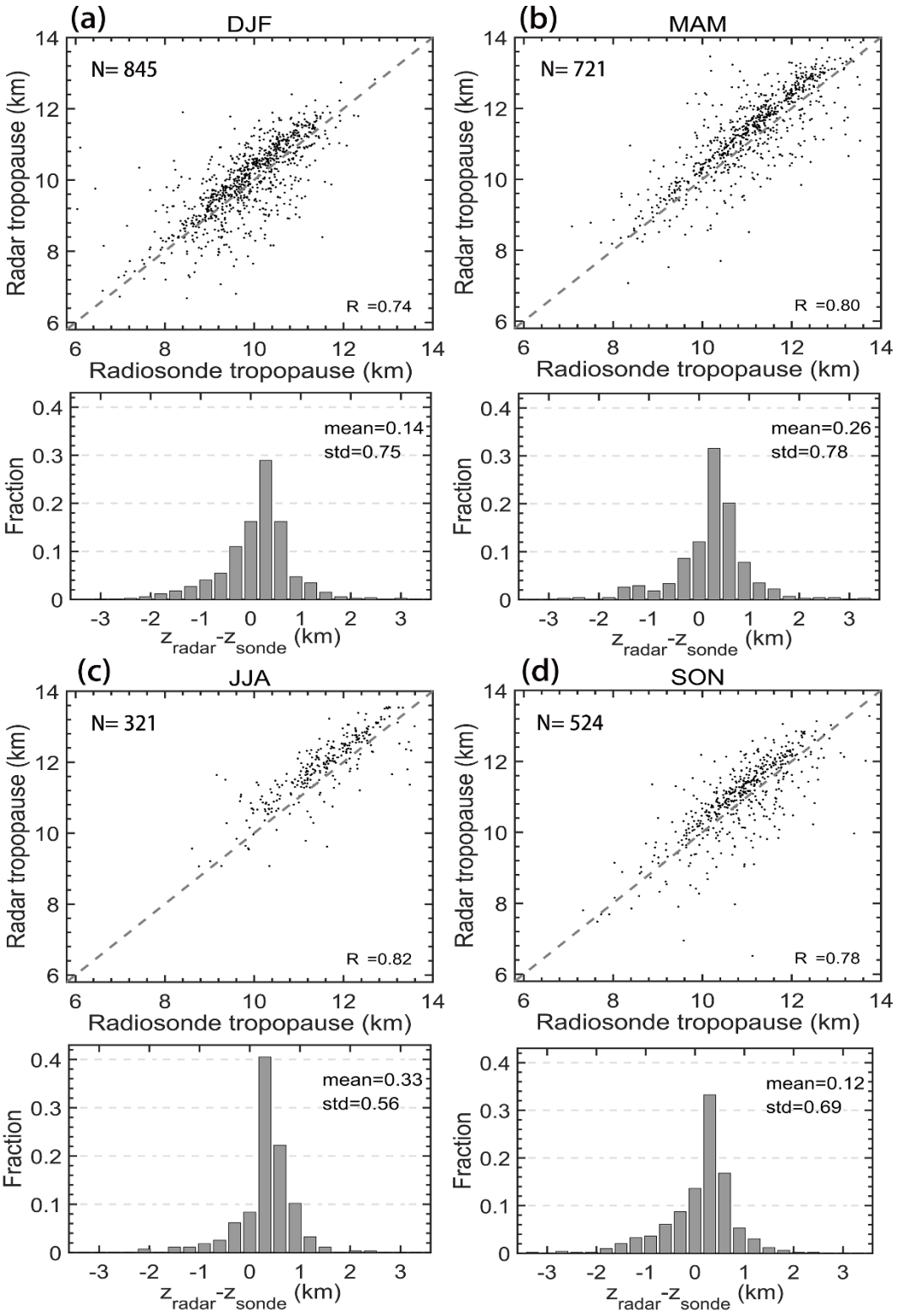

Figure 4. Seasonal scatterplots of the RT versus LRT and histogram distribution of altitude differences between the RT and the LRT, for (a) winter DJF, (b) spring MAM, (c) summer JJA, and (d) autumn SON, during the period November 2011-May 2017.

The positive values in the histogram indicate the RT locating at a higher level than the LRT. The grey dashed line shows the 1:1 line. Here, 'N','R^2', 'mean', and 'std' indicate the sample numbers, correlation coefficient, mean difference, and standard deviation of the difference, respectively.

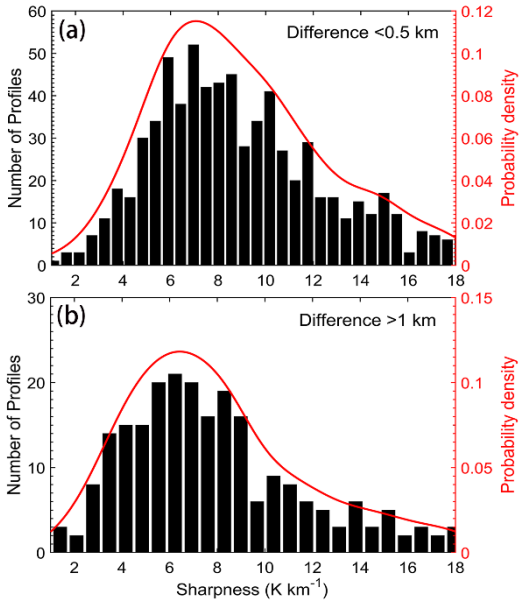

Figure 5. Histogram distribution of the tropopause sharpness for (a) difference <0.5 km, and (b) >1 km respectively between the LRT and the RT.

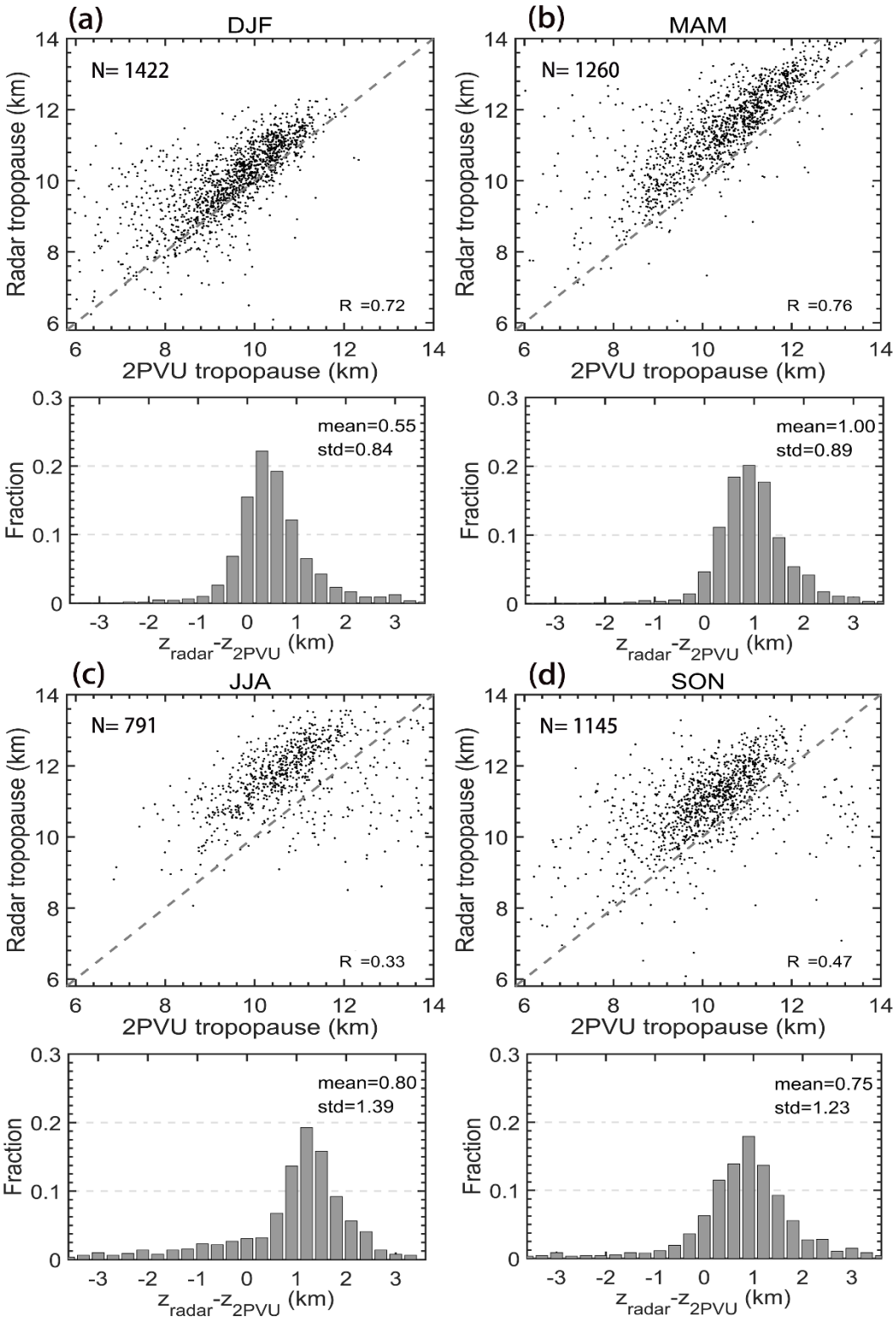

614

615 **Figure 6.** Same as figure 4, but for the comparison between the RT and the PVT.

616

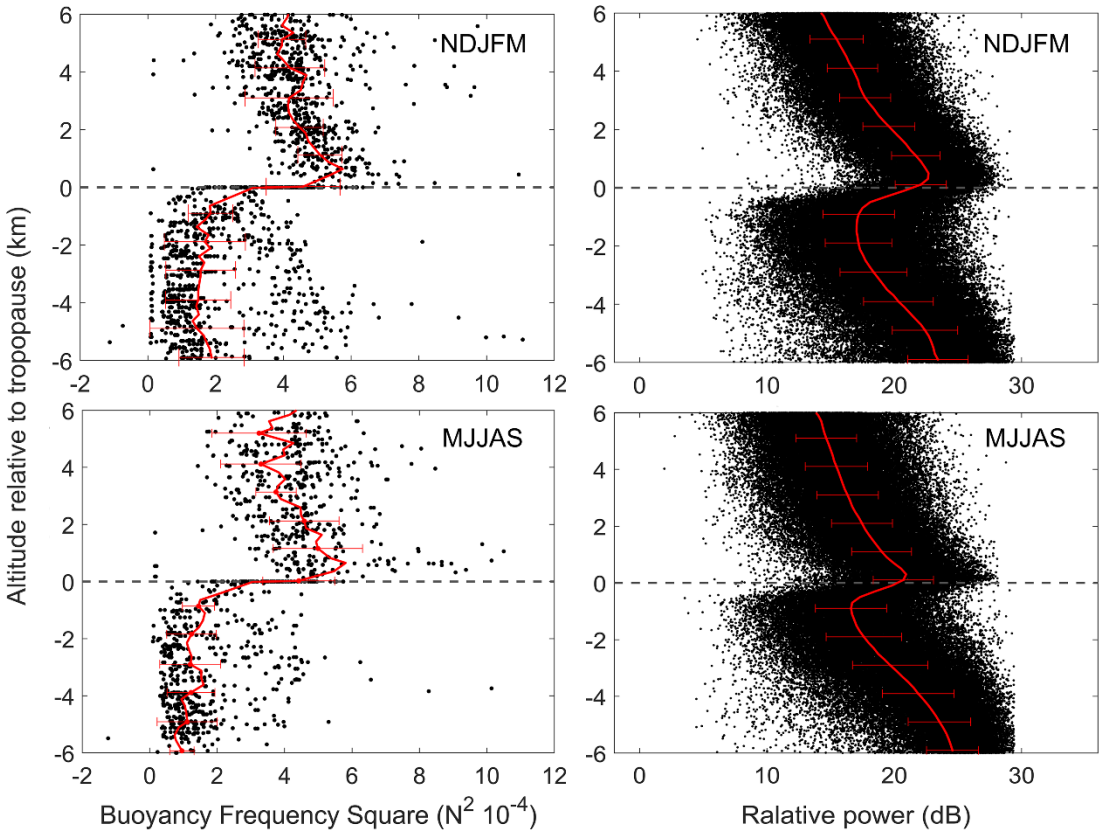

617

618 **Figure 7.** Scatterplots of (left panels) static stability (N^2) and (right panels) radar

619 relative echo power as a function of altitude relative to the LRT (left panels) and RT

620 (right panels) for extended winter (NDJFM) and summer (MJJAS) seasons for two

621 specific years 2012-2013. Red lines in each panel denote the corresponding mean

622 profiles and the error bars indicate the standard deviations.

623

624

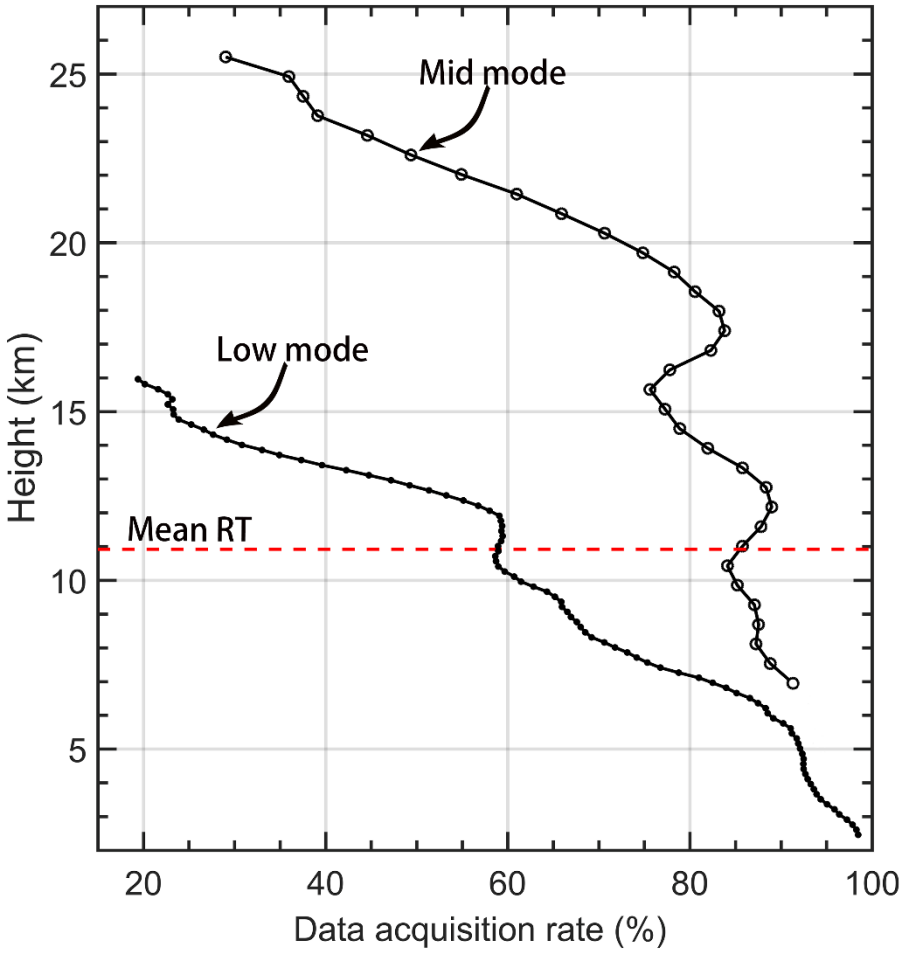

625

626 **Figure 8.** Vertical height profiles of the averaged effective radar wind data acquisition

627 rate in low mode and middle mode during November 2011-May 2017. The red dashed

628 line indicates the mean RT height.

629

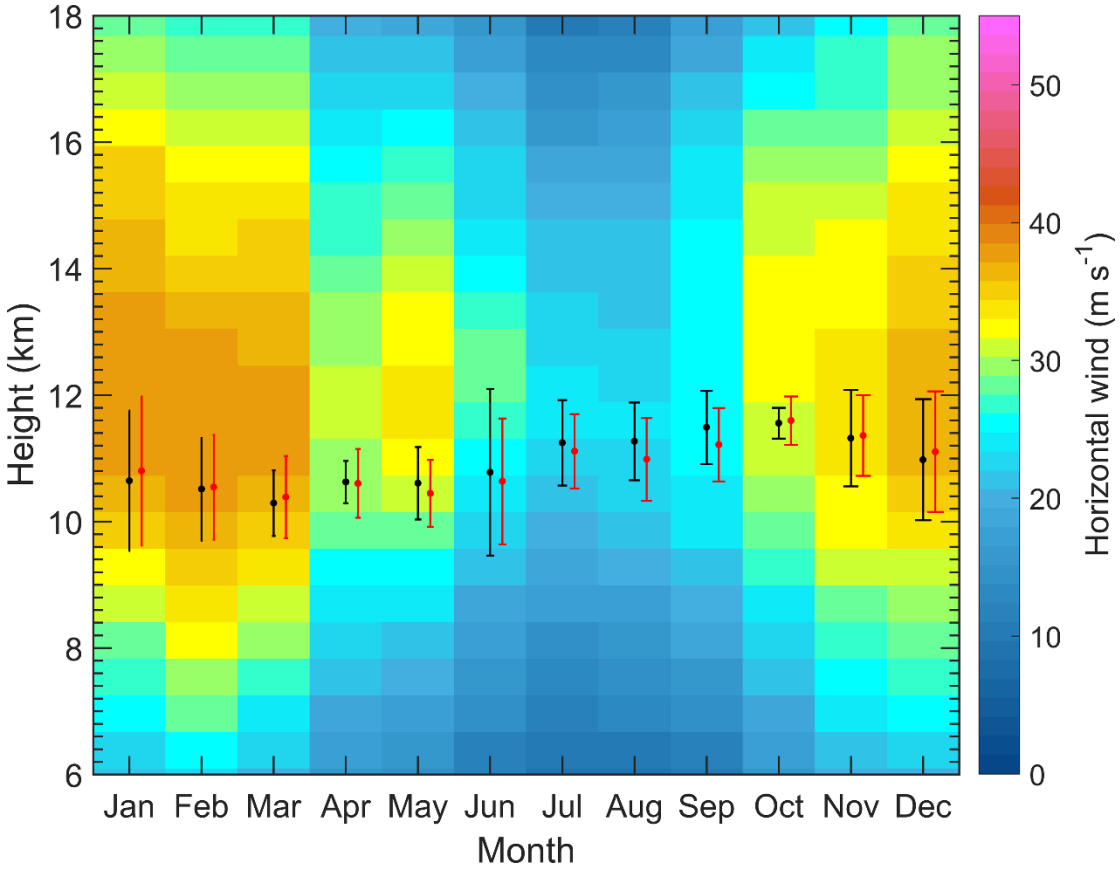

630

631 **Figure 9.** Height-time intensity map of monthly mean horizontal wind speed (shaded,

632 m/s) derived from the middle mode of Beijing MST radar, during November 2011-May

633 2017. Also shown is the monthly mean height of RT (black dots) and LRT (red dots,

634 offset by +6 days) along with the vertical error bars representing the standard deviations.

635

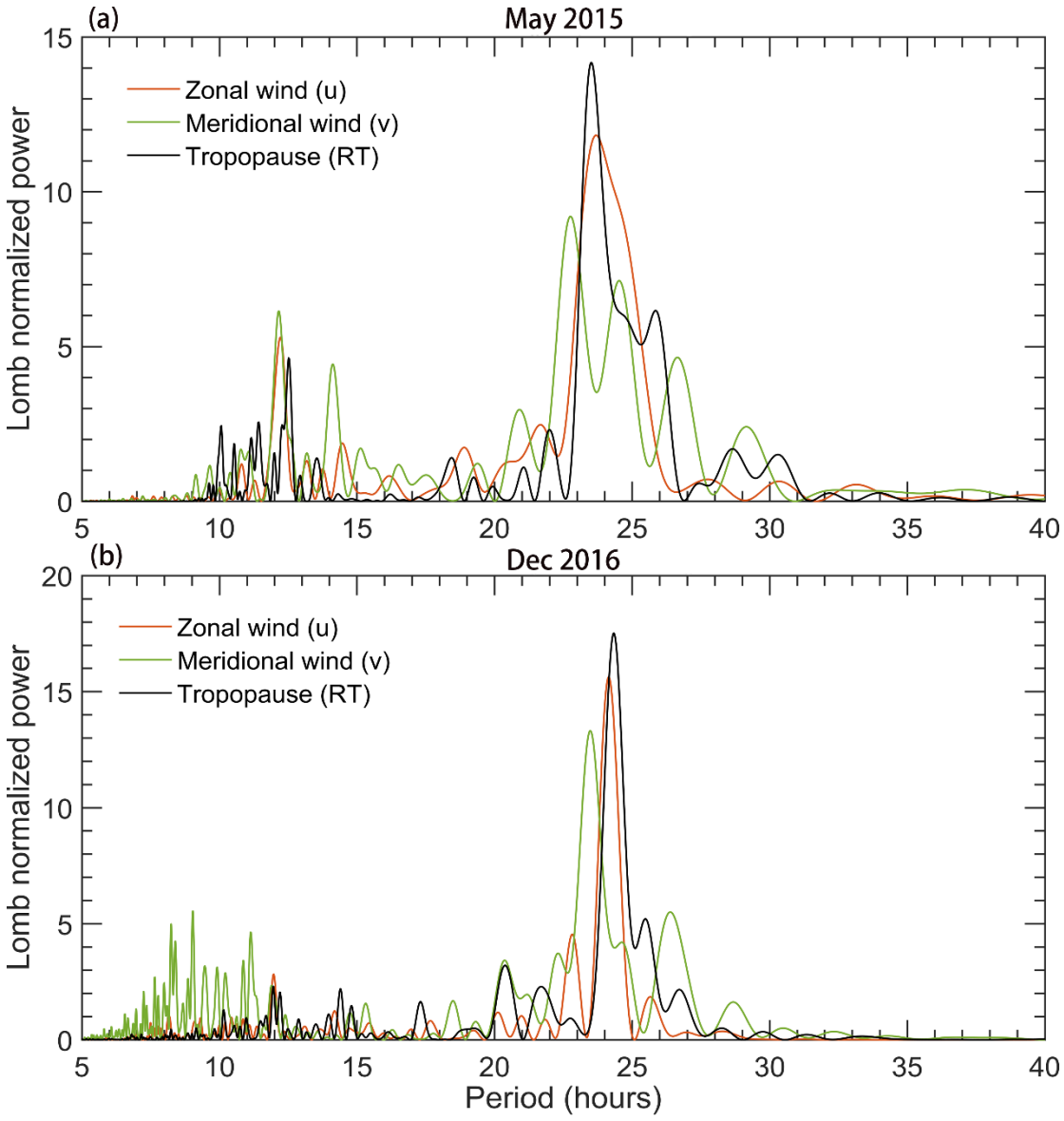

Figure 10. Lomb-Scargle periodograms of the RT height, zonal, and meridional wind oscillations for specific months of (a) May 2015 and (b) December 2016. The zonal and meridional wind for (a) is sampled at 9.85 km and (b) at 11 km.

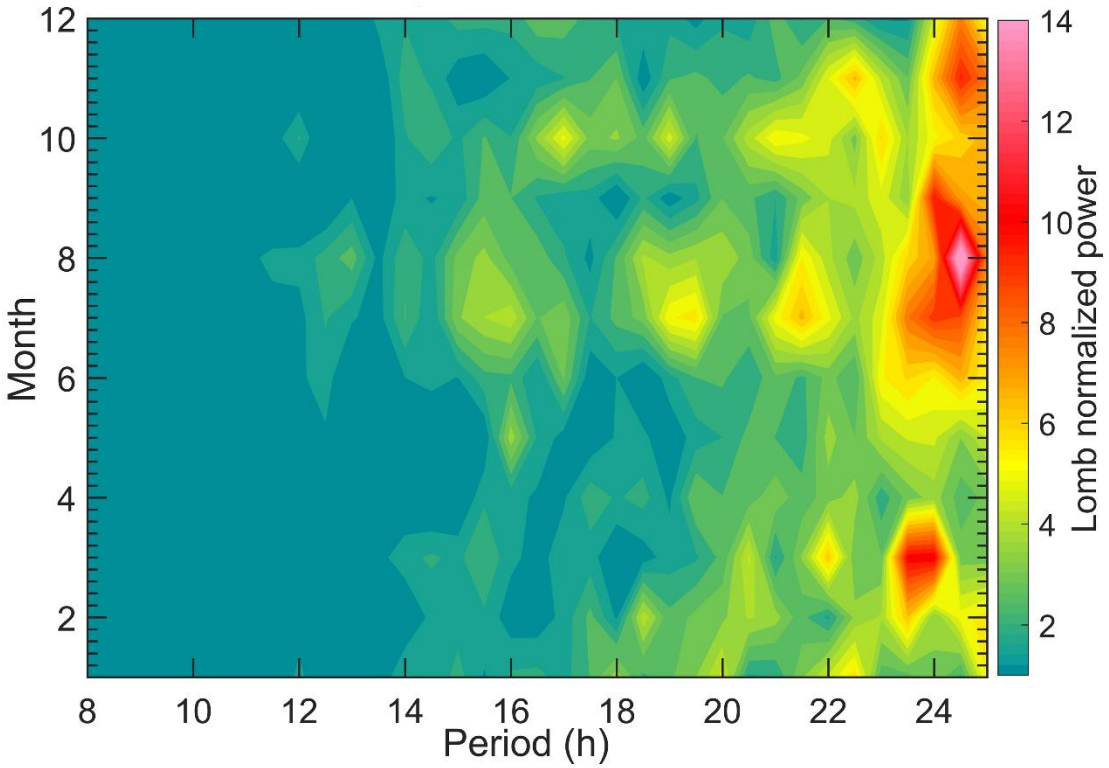

641

642 **Figure 11.** Mean Lomb-Scargle periodograms of RT height as a function of the time of

643 month during November 2011-May 2017.

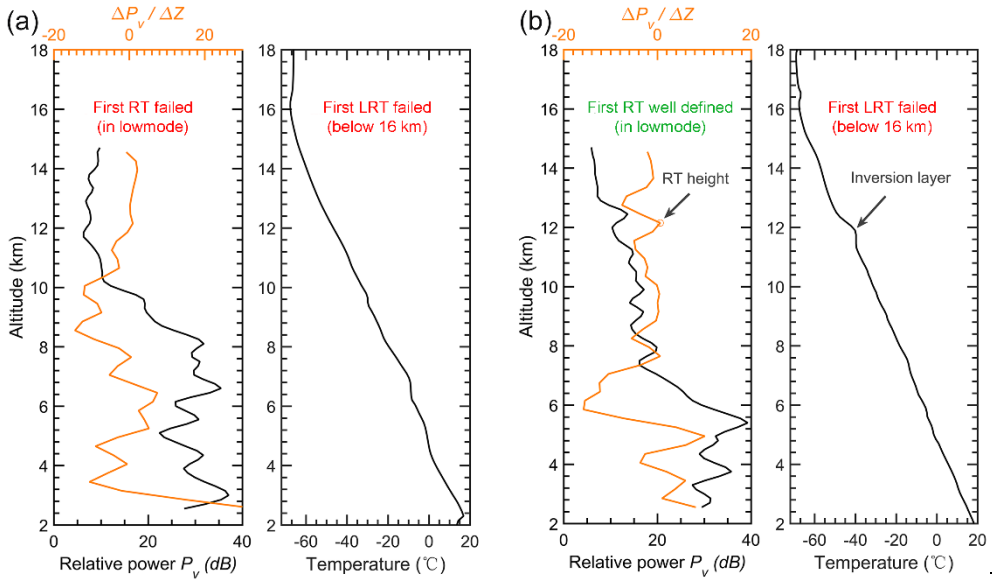

644

645 **Figure 12.** Example profiles of radar echo power and radiosonde temperature that (a)

646 both the RT and LRT definitions fail due to the continuing decrease in temperature on

647 00 UTC 7 July 2012 and (b) the temperature inversion layer failed to meet the LRT

648 definition but well defined in RT definition on 12 UTC 02 August 2012. Please note

that we only consider the conditions below 16 km.